Numerical study of $O(a)$ improved Wilson quark action on an anisotropic lattice

Hideo Matsufuru and Tetsuya Onogi
Yukawa Institute for Theoretical Physics, Kyoto University, Kyoto 606-8502, Japan

Takashi Umeda
Center for Computational Physics, University of Tsukuba, Tsukuba 305-8577, Japan

(Received 3 July 2001; published 5 November 2001)

The $O(a)$ improved Wilson quark action on the anisotropic lattice is investigated. We carry out numerical simulations in the quenched approximation at three values of lattice spacing ($a_\sigma^{-1}=1-2$ GeV) with the anisotropy $\xi=a_\sigma/a_\tau=4$, where a_σ and a_τ are the spatial and temporal lattice spacings, respectively. The bare anisotropy γ_F in the quark field action is numerically tuned by the dispersion relation of mesons so that the renormalized fermionic anisotropy coincides with that of the gauge field. This calibration of the bare anisotropy is performed to the level of 1% statistical accuracy in the quark mass region below the charm quark mass. The systematic uncertainty in the calibration is estimated by comparing the results from different types of dispersion relation, which gives 3% on our coarsest lattice and tends to vanish in the continuum limit. In the chiral limit, there is an additional systematic uncertainty of 1% from the chiral extrapolation. Taking the central value $\gamma_F=\gamma_F^*$ from the result of the calibration, we compute the light hadron spectrum. Our hadron spectrum is consistent with the result of the UKQCD Collaboration on the isotropic lattice. We also study the response of the hadron spectrum to a change of the anisotropic parameter $\gamma_F\to\gamma_F^*+\delta\gamma_F$. We find that a change of γ_F by 2% induces a change of 1% in the spectrum for physical quark masses. Thus the systematic uncertainty on the anisotropic lattice, as well as the statistical one, is under control.

DOI: 10.1103/PhysRevD.64.114503 PACS number(s): 11.15.Ha

I. INTRODUCTION

The anisotropic lattice is drawing more attention as a useful technique of lattice QCD simulation in various fields of physics, such as the spectroscopy of exotic states, finite temperature QCD, and heavy quark physics. However, the advantage of having a fine lattice spacing in the temporal direction is obtained at the sacrifice of manifest temporal-spatial axis interchange symmetry. Therefore improper use of the anisotropic lattice could lead to an unphysical result due to the lack of Lorentz symmetry in the continuum limit. This can be a serious problem for the physics in which the precision of the results is crucial.

One way to avoid this problem is to tune the anisotropy parameters of the action by imposing the conditions with which the Lorentz invariance is satisfied for some physical observables. In the Wilson plaquette gauge action there is only one anisotropic parameter in the action [1]. Wilson loops are used to obtain the relation between the anisotropic parameter and the physical ratio of the lattice spacings in temporal and spatial directions, $\xi=a_\sigma/a_\tau$, where a_σ and a_τ are the spatial and temporal lattice spacings [2–5]. On the other hand, not much is known about the quark action. This is because previous work on the quark action on the anisotropic lattice has been devoted to charmonium systems [6–9]. In order to apply the anisotropic lattice to systems containing light quarks, one has to study how one can tune the parameter of the light quark action in practical simulations.

In this paper we study the $O(a)$ improved Wilson action on the anisotropic lattice using quenched lattices with three lattice spacings, at fixed renormalized anisotropy $\xi=4$. These scales cover the range of the spatial lattice cutoff $a_\sigma^{-1}=1-2$ GeV. We first tune the bare anisotropy in the quark action numerically so that the renormalized fermionic anisotropy is equal to that of the gauge field, by imposing the relativistic dispersion relation of mesons. This calibration is performed to the level of 1% statistical accuracy in the whole quark mass region below the charm quark mass. The extrapolation of the tuned bare anisotropy to the chiral limit is performed by fitting to presumable forms, and causes additional systematic uncertainty of 1% at the chiral limit. The systematic uncertainty in the calibration from lattice artifacts is estimated by comparing the results from different types of dispersion relation. It results in 3% uncertainty on our coarsest lattice, and tends to vanish in the continuum limit. Using the result of the calibration we compute the light hadron spectrum on anisotropic lattices, and examine how the uncertainty in the calibration affects the spectrum for the parameters of physical interest. It is found that an uncertainty of 2% in calibration induces a systematic error of 1% in the spectrum. Thus the systematic uncertainty on the anisotropic lattice is under control, as well as the statistical one. We also show that anisotropic lattices produce results consistent with those on isotropic lattices, and that the Lorentz invariance of the simple matrix element is satisfied within errors.

This paper is organized as follows. The next section describes the $O(a)$ improved Wilson quark action, which has been discussed in [10,6]. The calibration procedures are discussed in Sec. III. In Sec. IV, we perform the calibration of the bare anisotropy in the quark action. The systematic uncertainty induced by this tuning is fully examined. In Sec. V we apply the anisotropic lattice to light hadron spectroscopy. In the last part of this section, the systematic uncertainty due to the anisotropy is again investigated in terms of the effect

on the hadron spectrum. The last section is devoted to our conclusions.

II. QUARK ACTION ON AN ANISOTROPIC LATTICE

A. Quark field action

We employ the $O(a)$ improved quark action on an anisotropic lattice. The form of action has been discussed in Ref. [10]; it is the same as the Fermilab action [11] but defined on an anisotropic lattice. In this section we summarize the results that will be necessary in the following calculations.

The quark action is represented in the hopping parameter form as

$$S_F=\sum_{x,y}\ \overline{\psi}(x)K(x,y)\psi(y), \tag{2.1}$$

$$\begin{aligned}K(x,y)=&\delta_{x,y}-\kappa_\tau[(1-\gamma_4)U_4(x)\delta_{x+\hat{4},y}+(1+\gamma_4)\\&\times U_4^\dagger(x-\hat{4})\delta_{x-\hat{4},y}]-\kappa_\sigma\sum_i\ [(r-\gamma_i)U_i(x)\\&\times\delta_{x+\hat{i},y}+(r+\gamma_i)U_i^\dagger(x-\hat{i})\delta_{x-\hat{i},y}]\\&-\kappa_\sigma c_E\sum_i\ \sigma_{4i}F_{4i}(x)\delta_{x,y}\\&-r\kappa_\sigma c_B\sum_{i>j}\ \sigma_{ij}F_{ij}(x)\delta_{x,y},\end{aligned} \tag{2.2}$$

where κ_σ and κ_τ are the spatial and temporal hopping parameters, r is the Wilson parameter, and c_E and c_B are the clover coefficients. In principle, for a given κ_σ, the four parameters $\kappa_\sigma/\kappa_\tau$, r, c_E, and c_B should be tuned so that Lorentz symmetry holds up to discretization errors of $O(a^2)$.

On an anisotropic lattice, the mean-field values of the spatial link variable u_σ and the temporal one u_τ are different from each other. The tadpole improvement [12] is achieved by rescaling the link variable as $U_i(x)\to U_i(x)/u_\sigma$ and $U_4(x)\to U_4(x)/u_\tau$. This is equivalent to redefining the hopping parameters as the tadpole-improved ones (with tilde) through $\kappa_\sigma=\tilde{\kappa}_\sigma/u_\sigma$ and $\kappa_\tau=\tilde{\kappa}_\tau/u_\tau$. We define the anisotropy parameter γ_F as

$$\gamma_F\equiv\frac{\tilde{\kappa}_\tau}{\tilde{\kappa}_\sigma}. \tag{2.3}$$

At the tadpole-improved tree level, and for sufficiently small quark mass, the anisotropy γ_F coincides with the cutoff anisotropy $\xi=a_\sigma/a_\tau$.

In this work, we set the coefficients of the spatial part of the Wilson term and the clover coefficients as the tadpole-improved tree-level values, namely,

$$r=\frac{1}{\xi},\qquad c_E=\frac{1}{u_\sigma u_\tau^2},\qquad c_B=\frac{1}{u_\sigma^3}, \tag{2.4}$$

and perform a nonperturbative calibration only for γ_F with the meson dispersion relation.

It is useful to define κ

$$\frac{1}{\kappa}\equiv\frac{1}{\tilde{\kappa}_\sigma}-2(\gamma_F+3r-4) \tag{2.5}$$

so that the bare quark mass in spatial lattice units, $m_{0\sigma}$ is expressed as

$$m_{0\sigma}=\frac{1}{2}\left(\frac{1}{\kappa}-8\right), \tag{2.6}$$

which is analogous to the value on an isotropic lattice.

B. Dispersion relation of free quark

In this subsection, we examine the dispersion relation of the free quark on an anisotropic lattice. First the tree-level relation of bare anisotropy with ξ is derived from the condition that the rest mass and the kinetic mass coincide. Then we discuss how the dispersion relation is distorted at the edge of the Brillouin zone due to our choice $r=1/\xi$ [6].

From the action (2.2), the free quark propagator satisfies the dispersion relation

$$\cosh E(\boldsymbol{p})=1+\frac{\overline{\boldsymbol{p}^2}+\left[m_0+\frac{1}{2}(r/\gamma_F)\hat{\boldsymbol{p}}^2\right]^2}{2\left[1+m_0+\frac{1}{2}(r/\gamma_F)\hat{\boldsymbol{p}}^2\right]}, \tag{2.7}$$

where $\overline{p_i}=(1/\gamma_F)\sin p_i$, $\hat{p}_i=2\sin(p_i/2)$, and $m_0=m_{0\sigma}/\gamma_F$ is the bare quark mass in temporal lattice units. Setting $\boldsymbol{p}=\boldsymbol{0}$, Eq. (2.7) gives the rest mass

$$M_1\equiv E(\boldsymbol{0})=\ln(1+m_0). \tag{2.8}$$

On the other hand, the kinetic mass is defined and obtained as

$$\frac{1}{M_2}\equiv\xi^2\left.\frac{d^2E}{dp_i^{\,2}}\right|_{\boldsymbol{p}=\boldsymbol{0}}=\xi^2\left(\frac{r/\gamma_F}{m_0+1}+\frac{2/\gamma_F^2}{m_0(m_0+2)}\right). \tag{2.9}$$

Generally the rest mass (2.8) and the kinetic mass (2.9) are different. One can tune the bare anisotropy parameter γ_F so that it gives the same values for the rest and kinetic masses [11]. Putting the rest and the kinetic masses equal, the anisotropy parameter γ_F is represented using m_0 and r as

$$\frac{1}{\gamma_F}=\sqrt{\left(\frac{rm_0(m_0+2)}{4(m_0+1)}\right)^2+\frac{m_0(m_0+2)}{2\xi^2\ln(1+m_0)}}-\frac{rm_0(m_0+2)}{4(m_0+1)}. \tag{2.10}$$

For small m_0, γ_F is expanded in m_0 as

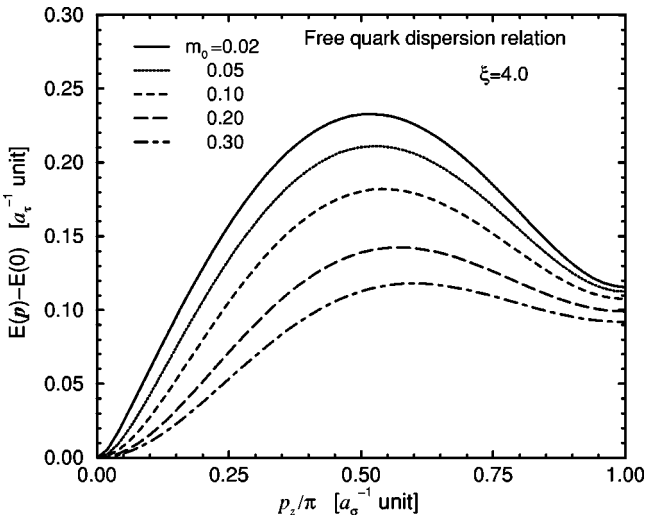

FIG. 1. Dispersion relation of the free quark for $\xi=4$.

$$\frac{1}{\gamma_F}=\frac{1}{\xi}\left[1+\frac{1}{2}(1-r\xi)m_0+\frac{1}{24}(-1+6r\xi+3r^2\xi^2)m_0^2\right]$$
$$=\frac{1}{\xi}\left[1+\frac{1}{3}m_0^2\right] \qquad (r=1/\xi). \tag{2.11}$$

The m_0 dependence starts with the quadratic term for $r=1/\xi$; therefore the dependence on the quark mass is small for sufficiently small m_0. For example, let us consider the case of $a_\tau=4$ GeV, which corresponds to the coarsest lattice in our simulation. The charm quark mass corresponds to $m_0\simeq 0.3$ and at this value γ_F is different from ξ by only 3%. Up to this quark mass region, one can expect that the difference of γ_F from ξ will also be small in the numerical simulation. This is examined in Sec. IV.

With our choice of Wilson parameter $r=1/\xi$, the action (2.2) leads to a smaller spatial Wilson term for a larger cutoff anisotropy ξ. The question is how the contribution of the doubler eliminated by the Wilson term becomes significant for practical values of ξ. In the following argument on this subject, we treat only the case of γ_F almost equal to ξ, i.e., the region of m_0 sufficiently smaller than unity. Figure 1 shows the dispersion relation (2.7) for several values of m_0 in the case of $\xi=4$, which we use in the numerical simulation.

Let us examine the practical case $a_\sigma^{-1}\simeq 1.0$ GeV, which corresponds to the lowest spatial cutoff of our three lattices. For the light quark mass region, $m_0=0.02$–0.05 corresponds to 80–200 MeV, and roughly covers the mass region that we use in the hadron spectroscopy in Sec. V. $E(\boldsymbol{p})-E(\boldsymbol{0})$ rapidly decreases at the edge of the Brillouin zone, and the height at $z=a/\pi$ is around 400 MeV. For two quarks with momenta $p=\pm a/\pi$, the additional energy of the doublers is $\sim$800 MeV, and is not expected to have a severe effect on the spectrum and other observables. For a higher lattice cutoff, the situation improves. Thus we regard the doubler contribution as sufficiently small on the lattice we use in the simulation. $m_0=0.3$ roughly corresponds to the charm quark mass with $a_\sigma^{-1}\simeq 1$ GeV. In the case of heavy-light hadrons, such as D mesons and Λ_c baryons, the scale of momentum transfer inside the hadrons is of the order of Λ_{QCD}, and the same argument holds as for the light quark case. On the other hand, for the heavy quarkonium, the typical energy and momentum exchanged inside the meson are on the order of mv^2 and mv, respectively [13]. For the charmonium, $v^2\sim 0.3$; thus the typical scale of the kinetic energy is around 500 MeV. This seems not sufficiently smaller than the two doublers' contributions, and hence one needs to choose a larger lattice cutoff in the calculation of the heavy quarkonium.

III. CALIBRATION PROCEDURES

On an anisotropic lattice, one must tune the parameters so that the anisotropy of the quark field, ξ_F, equals that of the gauge field, ξ_G:

$$\xi_F(\beta,\gamma_G;\kappa,\gamma_F)=\xi_G(\beta,\gamma_G;\kappa,\gamma_F)=\xi. \tag{3.1}$$

Since ξ_G and ξ_F are in general functions of both gauge parameters (β,γ_G) and quark parameters (κ,γ_F), a simulation with dynamical quarks requires tuning these bare parameters simultaneously. In the quenched case, however, this tuning is rather easy to perform, since ξ_G can be determined independently of γ_F. After the determination of ξ, one can tune γ_F so that a certain observable satisfies the condition (3.1). In this work, we use the relativistic dispersion relation of mesons

$$E^2(\boldsymbol{p})=m^2+\frac{\boldsymbol{p}^2}{\xi_F^2}+O(\boldsymbol{p}^4) \tag{3.2}$$

as our main calibration procedure. The energy and the mass of the meson, E and m, are in temporal lattice units while the momentum is in spatial lattice units. ξ_F appears to convert the momentum in spatial lattice units into temporal lattice units, and it is considered as the fermionic anisotropy defined through this relation. With the condition $\xi_F=\xi$, this condition satisfies the requirement that the rest mass and the kinetic mass one equal to each other. For finite lattice spacings, the above dispersion relation holds only up to the $O((\boldsymbol{p}^2)^2)$ correction term. In the continuum limit, this higher order term in a would vanish and the relativistic dispersion relation would be restored.

In the numerical simulation, we fit E^2 to the form Eq. (3.2) and obtain the value of ξ_F for each input value of the bare anisotropy γ_F. Then we linearly interpolate ξ_F in terms of γ_F and find γ_F^*, the value of γ_F for which $\xi_F=\xi$ holds.

In order to estimate the systematic errors we also use the dispersion relation that corresponds to the lattice Klein-Gordon action [6],

$$\cosh E(\boldsymbol{p})-\cosh E(\boldsymbol{p}=\boldsymbol{0})=\frac{1}{2\xi_{KG}^2}\hat{\boldsymbol{p}}^2. \tag{3.3}$$

Thus the comparison of these two calibration conditions typically shows the size of the lattice discretization errors.

Expanding this expression in a, ξ_{KG} is related to ξ_F as

TABLE I. Lattice parameters. The scale a_σ^{-1} is determined from the hadronic radius r_0. The mean-field values are in the Landau gauge. The statistical uncertainty of u_τ is less than the last digit.

β	γ_G	Size	r_0	a_σ^{-1} (GeV)	u_σ	u_τ	η_{MF}
5.75	3.072	$12^3\times 96$	2.786(15)	1.100(6)	0.7620(2)	0.9871	1.2953(4)
5.95	3.1586	$16^3\times 128$	4.110(23)	1.623(9)	0.7917(1)	0.9891	1.2494(2)
6.10	3.2108	$20^3\times 160$	5.140(32)	2.030(13)	0.8059(1)	0.9901	1.2285(2)

$$\xi_{KG}=\xi_F\left(1-\frac{m^2}{12}+O(a^4)\right). \tag{3.4}$$

The same input γ_F gives a smaller value for ξ_{KG} than for ξ_F, and therefore the tuned bare anisotropy γ_F^* results in a larger value in the former case.

IV. NUMERICAL RESULTS OF CALIBRATION

The goal of this section is to determine the tuned bare anisotropy of the quark field, γ_F^*, at each fixed quark mass in the region from strange to charm quark masses. The reason for this choice of the quark mass range is that the simulation is easier, which reduces the amount of work in the exhaustive study of the calibrations. Fitting the result as a function of the quark mass, we obtain γ_F^* to the statistical accuracy of the 1% level for the whole quark mass region below the charm quark mass, including the chiral limit.

Then we estimate the systematic uncertainties of γ_F^* which are mainly due to $O(\alpha a)$ and $O(a^2)$ lattice artifacts. We also investigate how these systematic errors as well as the statistical error affect the meson masses in the region $m_s<m_q<m_c$. The response of hadron masses with respect to γ_F in the light quark mass region, $m_q<m_s$, needs additional care, and is the subject of the next section. At the end of this section, we summarize the result of calibration.

A. Simulation parameters for the calibration

In this work, we use three lattices with $\beta=5.75$, 5.95, and 6.10 and renormalized anisotropy $\xi=4$. The value of γ_G corresponding to the desired value of ξ has been studied in detail by Klassen [5], and we can use his relation of γ_G and ξ which was obtained at 1% accuracy. The statistical uncertainties are, unless otherwise noted, estimated by the single elimination Jackknife method with appropriate binning. The configurations are separated by 2000 (1000) pseudo-heat-bath sweeps, after 20000 (10000) thermalization sweeps at $\beta=5.95$ and 6.10 (5.75). The configurations are fixed to the Coulomb gauge, which is particularly useful for the smearing of hadron operators.

The lattice cutoffs and the mean-field values of link variables are determined on smaller lattices with half the size in temporal extent for $\beta=5.75$ and 5.95, and otherwise with the same parameters, while at $\beta=6.10$ the lattice size is $16^3\times 64$. To obtain the lattice cutoffs, the static quark potential is measured by the standard procedure. We adopt the hadronic radius r_0 proposed by Sommer [14] to set the scale. Following the method in Ref. [14], we determine the force between static quark and antiquark, as a function of r_I, the interquark distance improved with the lattice one-gluon exchange potential form. Then we fit the values of the force, containing the off-axis data, to the form $\sigma+A/r_I^2$ in the fitting region roughly $0.5r_0<r_I<2r_0$. The parameters σ and A can be identified as the string tension and the Coulomb coefficient. The systematic uncertainty due to the choice of fit range is small, and at most the same size as the statistical error. Table I shows the values of r_0 and a_σ^{-1} determined by setting the physical value of r_0 as $r_0^{-1}=395$ MeV ($r_0\simeq 0.5$ fm). The quoted errors represent only the statistical uncertainty.

TABLE II. Calibration parameters and results at $\beta=5.75$. Linear fit is applied to the dispersion relation in the determination of ξ_F.

κ	Input γ_F	N_{conf}	$\gamma_F^{*(PS)}$	$\gamma_F^{*(V)}$	γ_F^*	$m_{PS}(\gamma_F^*)$	$m_V(\gamma_F^*)$
0.124	3.9,4.0	400	3.935(77)	3.83(18)	3.919(72)	0.1497(6)	0.2294(17)
0.122	3.9,4.0	400	3.904(48)	3.884(82)	3.899(45)	0.2044(4)	0.2650(12)
0.120	3.9,4.0	400	3.892(43)	3.888(54)	3.891(38)	0.2523(8)	0.3018(12)
0.118	3.9,4.0	400	3.906(36)	3.894(42)	3.901(31)	0.2967(9)	0.3387(12)
0.116	3.9,4.0	300	3.875(35)	3.841(42)	3.861(33)	0.3408(13)	0.3774(15)
0.114	3.9,4.0	200	3.899(36)	3.842(47)	3.878(36)	0.3819(17)	0.4142(19)
0.112	3.8,3.9,4.0	200	3.854(29)	3.806(37)	3.836(30)	0.4252(17)	0.4546(18)
0.110	3.8,3.9,4.0	200	3.878(33)	3.827(41)	3.857(34)	0.4654(22)	0.4918(23)
0.105	3.7,3.8,3.9,4.0	160	3.807(30)	3.754(37)	3.786(31)	0.5738(28)	0.5954(28)
0.101	3.7,3.8,3.9,4.0	160	3.730(26)	3.679(31)	3.709(27)	0.6653(30)	0.6845(30)
0.097	3.5,3.6	160	3.626(19)	3.587(24)	3.611(20)	0.7647(28)	0.7823(28)
0.095	3.5,3.6	160	3.579(18)	3.540(23)	3.564(19)	0.8166(29)	0.8333(29)
0.093	3.5,3.6	160	3.530(17)	3.490(21)	3.514(18)	0.8704(29)	0.8864(29)

TABLE III. Calibration parameters and results at $\beta=5.95$. Linear fit is applied to the dispersion relation in the determination of ξ_F.

κ	Input γ_F	N_{conf}	$\gamma_F^{*(PS)}$	$\gamma_F^{*(V)}$	γ_F^*	$m_{PS}(\gamma_F^*)$	$m_V(\gamma_F^*)$
0.124	3.9,4.0	500	4.073(95)	4.15(12)	4.103(80)	0.1177(6)	0.1649(9)
0.123	3.9,4.0	500	4.041(69)	4.095(93)	4.060(60)	0.1456(2)	0.1847(8)
0.122	3.9,4.0	500	4.029(55)	4.076(68)	4.048(48)	0.1712(4)	0.2045(8)
0.120	3.9,4.0	500	4.019(36)	3.996(55)	4.012(34)	0.2186(6)	0.2444(9)
0.118	3.9,4.0	500	4.003(29)	4.000(35)	4.002(28)	0.2625(8)	0.2841(9)
0.115	3.9,4.0	360	3.992(28)	3.969(36)	3.983(29)	0.3260(12)	0.3431(13)
0.110	3.9,4.0	300	3.945(28)	3.946(36)	3.946(29)	0.4297(19)	0.4427(19)
0.107	3.9,4.0	300	3.910(25)	3.911(31)	3.910(26)	0.4930(20)	0.5046(21)
0.104	3.9,4.0	200	3.876(28)	3.875(36)	3.876(30)	0.5573(27)	0.5677(27)
0.102	3.9,4.0	200	3.848(26)	3.847(34)	3.847(28)	0.6016(28)	0.6113(28)
0.100	3.9,4.0	200	3.815(25)	3.816(32)	3.815(27)	0.6470(29)	0.6562(29)
0.097	3.8,3.9	200	3.766(24)	3.765(30)	3.766(26)	0.7178(32)	0.7264(32)
0.093	3.7,3.8	200	3.688(23)	3.687(29)	3.688(25)	0.8180(37)	0.8257(37)

The mean-field values u_σ and u_τ are obtained as the average of the link variables in the Landau gauge, where the mean-field values are used self-consistently in the fixing condition [6]. These results are also listed in Table I. The mean-field value of the temporal gauge field has a small error and is close to unity. $\eta_{MF}=u_\tau/u_\sigma$, the mean-field estimate of $\eta=\xi/\gamma_G$, is close to the value of η determined nonperturbatively by Klassen. This suggests that the tadpole improvement works well on the anisotropic lattice also.

B. Quark field calibration

As described in Sec. III, we use the relativistic dispersion relation in the calibration of parameters in the quark action. Since the gauge field calibration is at the accuracy of 1%, we aim to tune the quark parameters to a similar level.

For convenience, we choose κ and γ_F as the input parameters and determine κ_σ and κ_τ from Eq. (2.5). Fixing κ corresponds to fixing the bare quark mass in spatial lattice units. For each value of (κ,γ_F), the pseudoscalar and vector meson correlators are obtained with zero and finite momenta. The fermionic anisotropy ξ_F is defined through the relativistic dispersion relation Eq. (3.2). We assume a linear dependence of ξ_F on γ_F in the vicinity of $\xi_F\simeq\xi$. We use linear interpolation to obtain γ_F^*, the value of γ_F at which the relation $\xi_F=\xi$ holds.

Result for the dispersion relation

The parameters (κ,γ_F) used in the calibration are listed in Tables II, III, and IV for $\beta=5.75$, 5.95, and 6.10, respectively. As the meson operators at the source, we adopt the smeared operators with appropriate smearing functions. For the light quark region, a Gaussian function is used as the smearing function, with a width of 0.2–0.4 fm. In the charm quark mass region, we also use the measured wave function for the smearing function. We measure the two-point functions for momenta $\boldsymbol{p}=\boldsymbol{n}(2\pi/L)$, where L is the spatial lattice extent and $\boldsymbol{n}=(0,0,0)$, $(1,0,0)$, $(1,1,0)$, $(1,1,1)$, and $(2,0,0)$.

TABLE IV. Calibration parameters and results at $\beta=6.10$. For $\kappa=0.124$, 0.123, and 0.122, the dispersion relation is fitted to a linear form in determining ξ_F. For the remaining κ's, a quadratic fit is applied.

κ	Input γ_F	N_{conf}	$\gamma_F^{*(PS)}$	$\gamma_F^{*(V)}$	γ_F^*	$m_{PS}(\gamma_F^*)$	$m_V(\gamma_F^*)$
0.124	4.0,4.1	600	4.020(77)	3.63(27)	3.991(79)	0.1008(5)	0.1379(7)
0.123	4.0,4.1	600	4.005(52)	3.860(98)	3.973(55)	0.1294(1)	0.1582(5)
0.122	4.0,4.1	600	3.998(41)	3.913(69)	3.976(44)	0.1549(3)	0.1787(6)
0.120	4.0,4.1	400	4.040(29)	4.064(45)	4.047(30)	0.2007(6)	0.2182(7)
0.118	4.0,4.1	200	4.040(33)	4.014(52)	4.032(34)	0.2440(9)	0.2579(10)
0.115	4.0,4.1	200	4.024(28)	4.008(41)	4.019(30)	0.3067(12)	0.3176(13)
0.110	4.0,4.1	200	4.013(38)	3.996(54)	4.007(43)	0.4078(26)	0.4160(27)
0.107	4.0,4.1	200	3.988(36)	3.986(46)	3.987(39)	0.4694(29)	0.4766(30)
0.104	4.0,4.1	200	3.951(33)	3.955(42)	3.952(36)	0.5331(31)	0.5396(31)
0.102	3.9,4.0	200	3.918(32)	3.928(40)	3.922(35)	0.5773(34)	0.5834(34)
0.100	3.9,4.0	200	3.877(25)	3.883(32)	3.879(27)	0.6240(28)	0.6298(28)
0.097	3.9,4.0	200	3.834(22)	3.839(28)	3.836(24)	0.6931(28)	0.6984(28)
0.093	3.8,3.9	200	3.769(21)	3.776(26)	3.772(23)	0.7903(32)	0.7953(31)

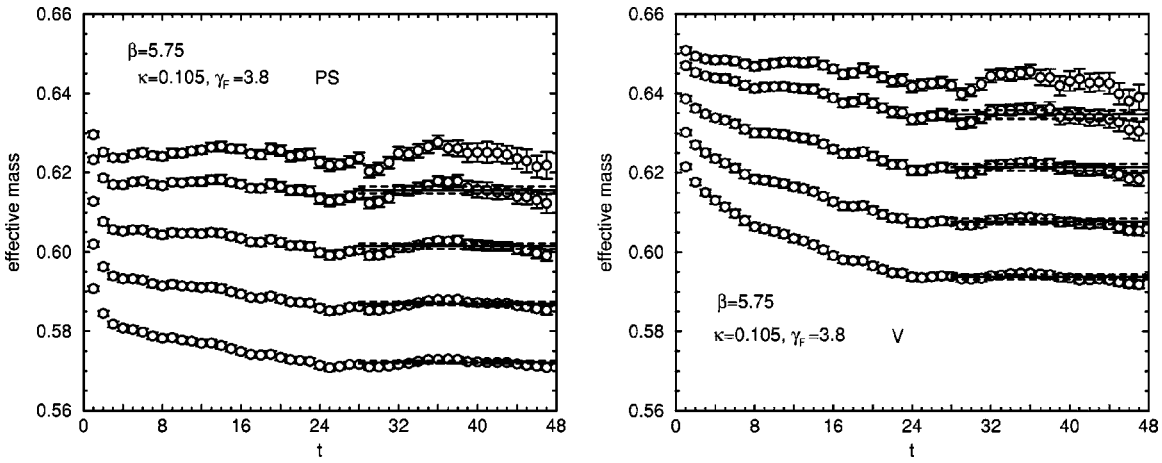

FIG. 2. Effective mass plots of PS and V mesons at $\kappa=0.105$, $\gamma_F=3.8$ on a $\beta=5.75$ lattice. From bottom to top, states with integer momentum vectors $\boldsymbol{n}=(0,0,0)$, $(1,0,0)$, $(1,1,0)$, $(1,1,1)$, and $(2,0,0)$. Horizontal solid lines represent the results of fits of correlators and the fitting range. The statistical errors are represented by the dashed lines. The state with $\boldsymbol{n}=(2,0,0)$ is not used in the fit of the dispersion relation at this β.

All rotationally equivalent $\boldsymbol{n}$'s are averaged. The standard procedure is used in extracting the energy at each momentum.

The energies are then fitted to linear or quadratic forms in $\boldsymbol{p}^2$ to extract the fermionic anisotropy ξ_F in each channel. In the case of a linear fit, we use only the three lowest momentum states $\boldsymbol{n}=(0,0,0)$, $(1,0,0)$, and $(1,1,0)$. We assume a linear dependence of $\xi_F(\gamma_F)$ on γ_F, and this is indeed verified in several examples.

Figure 2 shows typical effective mass plots for the pseudoscalar (PS) and vector (V) mesons. The energies of finite momentum states are successfully extracted from the region in which the correlator shows plateaus, except for the lightest quark region, $\kappa \geqslant 0.120$, which suffers severely from statistical fluctuation.

The dispersion relation for $\kappa=0.105$ at $\beta=5.75$ is shown in the left panel of Fig. 3. Because of the rather large lattice artifact, the fit to the quadratic form in $\boldsymbol{p}^2$ with the energy of the $\boldsymbol{n}=(2,0,0)$ state is not a good description of the data. We therefore use only the four lowest energy states in the quadratic fit. On the other hand, the results of the linear fit (with the lowest three states) and the quadratic fit coincide with good accuracy. For the few largest hopping parameters, the higher momentum states suffer such large statistical fluctuations that we always adopt the linear fit. Since at other values of κ the resultant ξ_F coincides with that of the quadratic fit, we adopt the linear fit for all values of κ at this β. Since the same method is adopted at $\beta=5.95$ at as $\beta=5.75$, we do not repeat the explanation for the fitting procedure.

The right panel of Fig. 3 shows the dispersion relation of mesons at $\beta=6.10$ and $\kappa=0.115$, which corresponds to a similar quark mass as $\kappa=0.105$ at $\beta=5.75$. The dispersion relation is much improved, and the quadratic fit is successfully applied including the $\boldsymbol{n}=(2,0,0)$ state. Although the difference from the linear fit is small, as shown in the figure, we adopt the result of the quadratic fit to determine ξ_F except for the lightest quark region. For these three largest κ, correlators with $\boldsymbol{n}=(2,0,0)$, and occasionally $(1,1,1)$, suffer

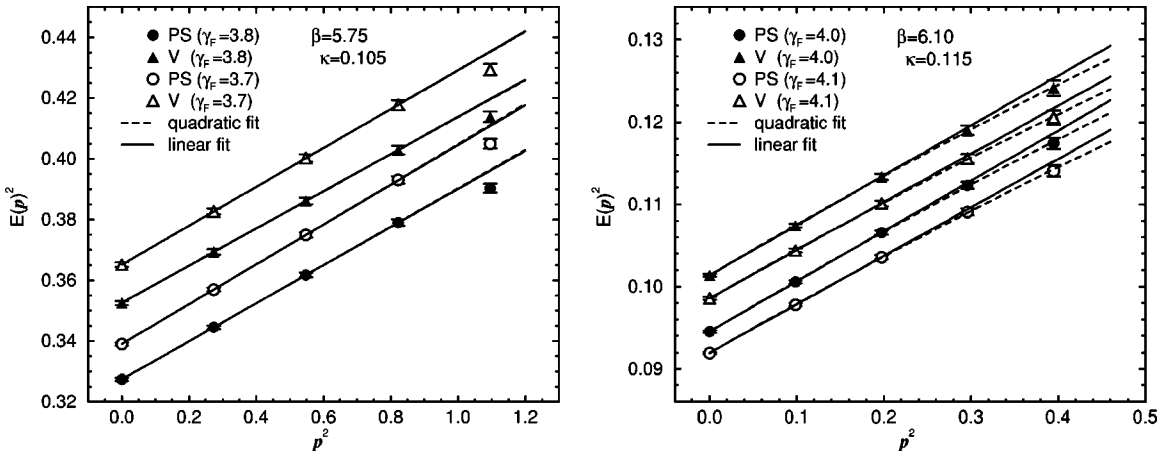

FIG. 3. Dispersion relations of PS and V mesons. The left panel shows the data at $\kappa=0.105$ and $\gamma_F=3.8$ and 3.7 on the $\beta=5.75$ lattice. The right panel shows the data at $\kappa=0.115$ and $\gamma_F=4.0$ and 4.1 on the $\beta=6.10$ lattice. Solid lines represent the linear fit and the dashed lines show the quadratic fit.

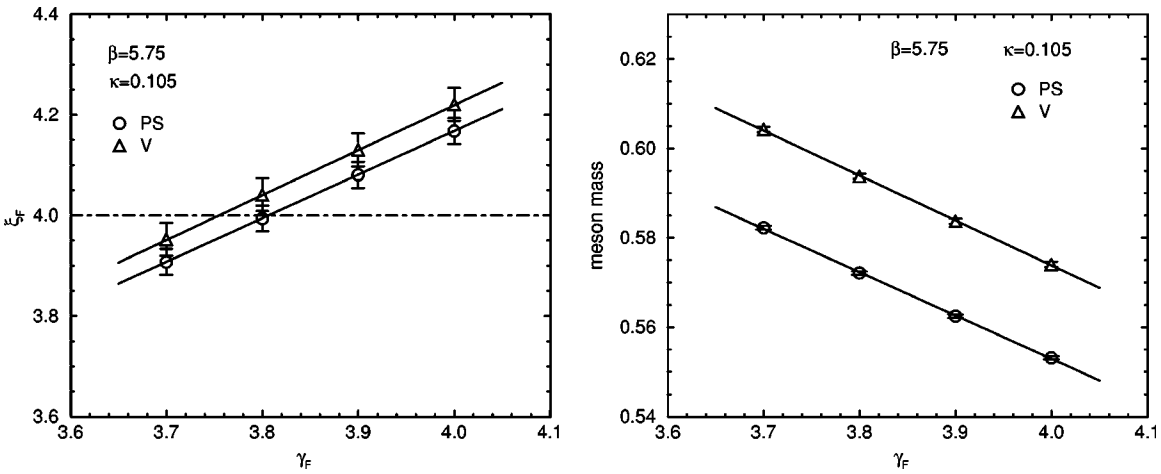

FIG. 4. γ_F dependence of ξ_F (left) and meson masses (right) at $\kappa=0.105$ on the $\beta=5.75$ lattice.

from such large statistical fluctuations that the energy of the states cannot be reliably extracted. In these cases, we fitted the energy to the linear form.

Calibration of γ_F for each quark mass

In the left panel of Fig. 4, ξ_F is plotted as a function of γ_F for $\kappa=0.105$ at $\beta=5.75$. It is clear that ξ_F depends linearly on γ_F. The results at $\kappa=0.101$, 0.110, and 0.112 show similar behavior. We therefore assume linear dependence also for other values of κ, and interpolate ξ_F to find γ_F^* in each channel. The numerical results for $\gamma_F^{*(PS)}$, $\gamma_F^{*(V)}$, and γ_F^* averaged over PS and V mesons are listed in Tables II–IV for each β. These tables also show the interpolated masses of PS and V mesons. We find a tendency for $\gamma_F^{*(PS)}$ to be slightly larger than $\gamma_F^{*(V)}$ in the whole κ region. This deviation seems to become smaller for larger β. The reason for the discrepancy is understood to be the systematic errors of $O(\alpha a)$, which will be examined in detail in the next subsection.

We also plot the γ_F dependence of the meson masses at $\kappa=0.105$ and $\beta=5.75$ in the right panel of Fig. 4. This shows that the meson mass is linear in γ_F in this range, and linear interpolation can be applied successfully to determine the meson masses at γ_F^*. Although the γ_F dependence of the meson mass is in general unknown for other regions of κ, we expect that the linear interpolation will work with good accuracy. The meson masses at γ_F^* are also listed in Tables II–IV for each β. How the uncertainty in γ_F^* affects the spectrum is an important problem, which will be examined in the next subsection.

Fit of γ_F^*

To represent γ_F^* as a function of κ, we introduce the quark mass as

$$m_q=\frac{1}{2\xi}\left(\frac{1}{\kappa}-\frac{1}{\kappa_c}\right). \tag{4.1}$$

This is similar relation as for m_0, the bare quark mass in temporal lattice units, while the present form is independent of γ_F. κ_c is determined from the massless point of the pseudoscalar meson mass. We extrapolate m_{PS}^2 linearly in $1/\kappa$ using the two largest values of κ, and find $\kappa_c=0.12640(5)$ at $\beta=5.75$, 0.12592(6) at $\beta=5.95$, and 0.12558(4) at $\beta=6.10$.

In the calibration at each κ, we found that the value of γ_F^* is easily determined precisely (to the level of 1%), while it becomes more difficult as κ increases toward κ_c. However, it is expected that γ_F^* smoothly approaches a certain definite value in the limit of $m_q\to 0$, since in this limit our form of action is simply a direct generalization of the clover quark action on an anisotropic lattice. In fact, as shown in Sec. II B, γ_F^* depends linearly on m_0^2 at the tree level. In taking the limit of $m_q\to 0$ for γ_F^*, the precise mean-field values do not matter, since in the definition of γ_F tadpole improvement is applied as a multiplicative factor, $\eta_{MF}=u_\tau/u_\sigma$. Therefore

TABLE V. Fit results for γ_F^*.

β	Fit type	ζ_0	ζ_1	ζ_2	χ^2/N_{df}	$\gamma_F^*(m_q=0)$
5.75	linear	0.2558(9)	–	0.230(12)	1.83 / 11	3.909(14)
	quad.	0.2564(23)	−0.007(28)	0.247(68)	1.77 / 10	3.901(34)
5.95	linear	0.2490(8)	–	0.189(15)	3.52 / 11	4.016(13)
	quad.	0.2465(18)	0.036(23)	0.095(61)	1.01 / 10	4.057(30)
6.10	linear	0.2479(9)	–	0.143(14)	4.44 / 11	4.034(14)
	quad.	0.2493(18)	−0.022(24)	0.200(63)	3.55 / 10	4.011(28)

the most reliable way to determine the value of γ_F^* in the light quark region is a global fit of γ_F^*, assuming the appropriate form of m_q dependence.

We fit the result of $1/\gamma_F^*$ to a linear form in m_q^2 and a quadratic form in m_q. The result of the fits is listed in Table V and also shown in Fig. 5 as the solid and the dashed curves. Since the points obtained for γ_F^* are with different numbers of configurations, these points do not correlate in an obvious way. We quote the errors and χ^2 of the uncorrelated fit in Table V. As shown in this table and figure, the linear fit in m_q^2 well represents the data. The value of ζ_0, which is $1/\gamma_F^*$ in the chiral limit, is close to the tree-level result $1/\xi = 1/4$, which implies that the tadpole improvement works well. Apart from the lightest quark mass region, γ_F^* is determined within 1% accuracy, and there the curves of the two fits are consistent with each other. In approaching the chiral limit, there is a systematic error concerning the fit form, as well as the statistical error. We estimate the latter by the error of the fit in ζ_0 (from the quadratic fit in m_q^2), to be about 1%. This relatively small statistical error is due to the global fit of $1/\gamma_F^*$ with the assumed form of m_q dependence. The systematic error in adopting a specific form of fit is estimated by the difference between these two fits, and is also at the 1% level. Adopting the linear form in m_q^2, we conclude that γ_F^* is determined under the assumed dispersion relation within 1% statistical accuracy in the whole quark mass region below the charm quark mass, while in the chiral limit there is an additional 1% systematic uncertainty concerning the form of the fit.

C. Uncertainties in calibration

In the last subsection, we determined γ_F^* as a global function of m_q. This expression inevitably suffers from systematic uncertainties as well as the statistical uncertainty:

$$\gamma_F^* = \gamma_F^{*(prop)} + \delta\gamma_F^{(stat)} + \delta\gamma_F^{[O(\alpha a)]} + \delta\gamma_F^{[O(a^2)]} (+ \delta\gamma_F^{(chiral)}). \tag{4.2}$$

$\gamma_F^{*(prop)}$ represents the proper value of the bare anisotropy. $\delta\gamma_F^{(stat)}$ is the statistical error in determination of γ_F^*, and is at the 1% level. The last two terms are the main sources of systematic errors due to finite lattice artifacts. The first one, $\delta\gamma_F^{[O(\alpha a)]}$, is from the tree-level approximation of the clover coefficients. We estimate the size of this error by the difference between the values of γ_F^* determined with PS and V mesons. The second systematic error, $\delta\gamma_F^{[O(a^2)]}$, is estimated by comparing the results of the calibration from two different forms of the dispersion relation that differ by $O(a^2)$. In addition to these systematic uncertainties, in the chiral limit there is also a systematic error concerning the form of the fit of γ_F^* in m_q.

Another important subject is to estimate how the observables are affected by the uncertainty in γ_F^*. We study the response of meson masses with respect to the change of γ_F^* at each κ, from which the effect of γ_F on the meson masses for a given quark mass is approximately estimated. Strictly speaking, changing γ_F for a fixed κ induces a slight change in the quark mass; hence the above analysis is adequate for the relatively heavier quark mass region, such as $m_s < m_q$. We postpone the study of the effect on the light hadron spectrum to the end of the next section.

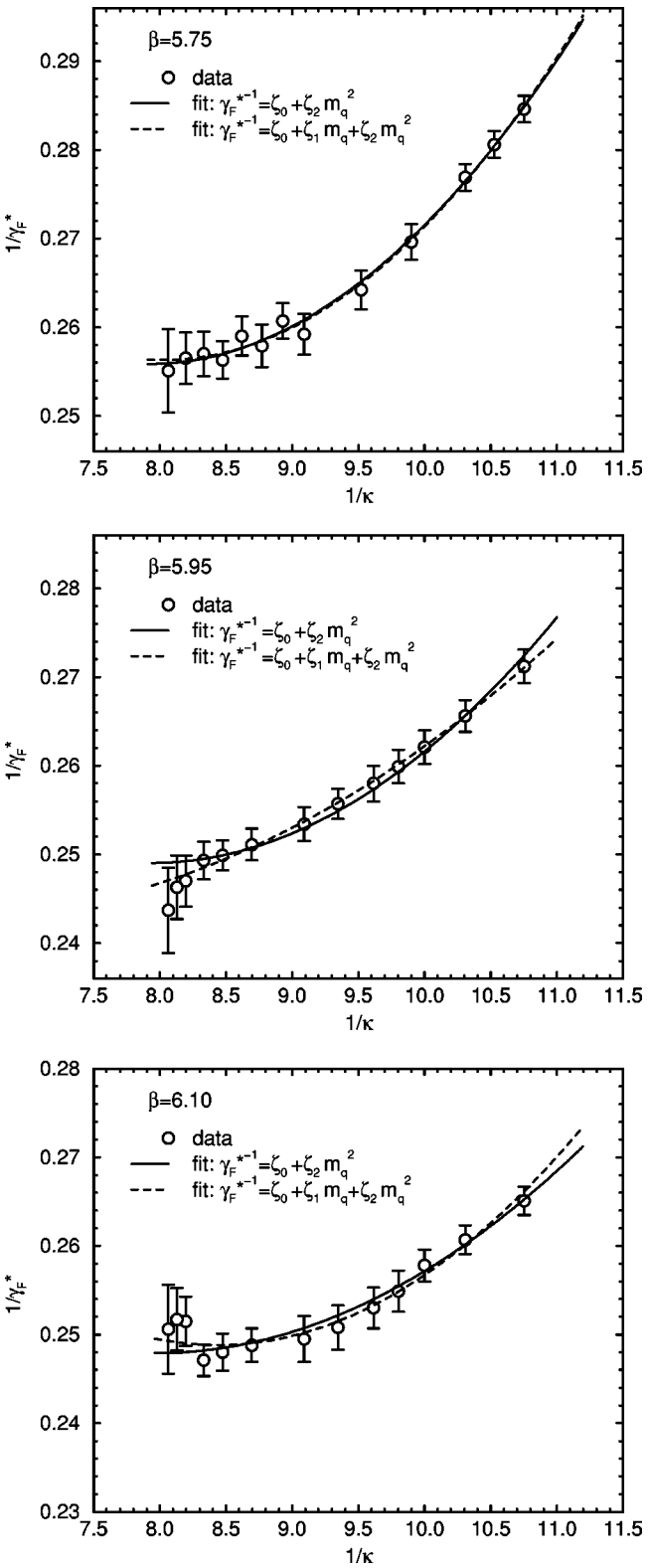

FIG. 5. $1/\gamma_F^*$ vs $1/\kappa$ at each β. Solid lines show the fit linear in m_q^2 while the dashed lines represent the fit quadratic in m_q.

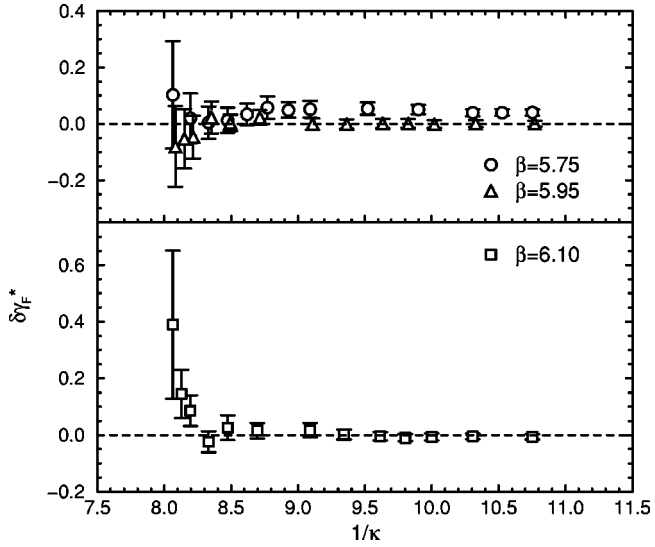

FIG. 6. $\delta\gamma_F^* = \gamma_F^{*(PS)} - \gamma_F^{*(V)}$ at $\beta = 5.75$ and 5.95 in the upper part and 6.10 in the lower part.

Difference between $\gamma_F^{*(PS)}$ and $\gamma_F^{*(V)}$

Since we use the $O(a)$-improved quark action, the main contribution from the $O(a)$ lattice artifact is absent. However, since the clover coefficients are not tuned beyond the tree level, the $O(\alpha a)$ error still remains, although the tadpole improvement partially removes this effect. An appropriate probe of this systematic effect on the calibration is the difference between the γ_F^*'s of the pseudoscalar and vector mesons. Figure 6 shows $\delta\gamma_F^* \equiv \gamma_F^{*(PS)} - \gamma_F^{*(V)}$. At $\beta = 5.75$, there is a systematic difference of $\delta\gamma_F^*$ from zero except in the small quark mass region, where the statistical error is dominant. At $\beta = 5.95$, $\delta\gamma_F^*$ is consistent with zero in the whole κ region. This implies that the $O(\alpha a)$ error in the calibration is sufficiently reduced at this β. In the case of $\beta = 6.10$, $\delta\gamma_F^*$ is also consistent with zero except in the lightest quark region. In this region, precise determination of the energy in finite momentum states is difficult due to the statistical fluctuation and hence the resultant γ_F^* contains a large uncertainty. We assume that the $O(\alpha a)$ effect in the calibration is also small at this β.

$O(a^2)$ systematic uncertainty

Although we employed the continuum dispersion relation, this introduces a systematic error of $O(a^2)$ to the calibration of γ_F. In order to estimate the typical size of this error, we compare γ_F^* determined above with $\gamma_{F(KG)}^*$, the result obtained using the dispersion relation from the lattice Klein-Gordon action, Eq. (3.3). Figure 7 shows this comparison at $\beta = 5.75$ and 6.10. In extracting ξ_{KG} from the Klein-Gordon dispersion relation, we fit $\cosh E(\boldsymbol{p})$ to a linear form in $\Sigma_i \sin^2(p_i/2)$ using the three lowest momentum states. As explained in Sec. III, the expected difference of ξ_F and ξ_{KG} is $O(m^2)$, where m is the meson mass. Although the explicit relation between $\gamma_{F(KG)}^*$ and γ_F^* is unknown, one can expect that the difference between them is also $O(m^2)$, and hence will increase with increasing quark mass. This behavior is clearly observed in Fig. 7. Table VI is the result of the fit of $\gamma_{F(KG)}^*$ to a linear form in m_q^2.

We find a small difference between the results with the relativistic and Klein-Gordon dispersion relations in the small quark mass region. This difference decreases with increasing β, and seems to be sufficiently reduced at $\beta = 6.10$. The typical size of the difference in γ_F^*'s at the chiral limit is less than 3%, 2%, and 1% at $\beta = 5.75$, 5.95, and 6.10, respectively. The important feature is that the two procedures tend to coincide with each other with increasing β. We also observe that the difference between γ_F^* and $\gamma_{F(KG)}^*$ increases in the large quark mass region, $m_q > 0.2 a_\tau^{-1}$. This is consistent behavior, since there the Klein-Gordon dispersion relation fails to incorporate the quark mass dependence properly, and $\gamma_{F(KG)}^*$ is expected to be larger than γ_F^* at $O(m^2)$. Therefore we conclude that the uncertainty due to the assumed form of the meson dispersion relation is under control and smoothly disappears on approaching the continuum limit.

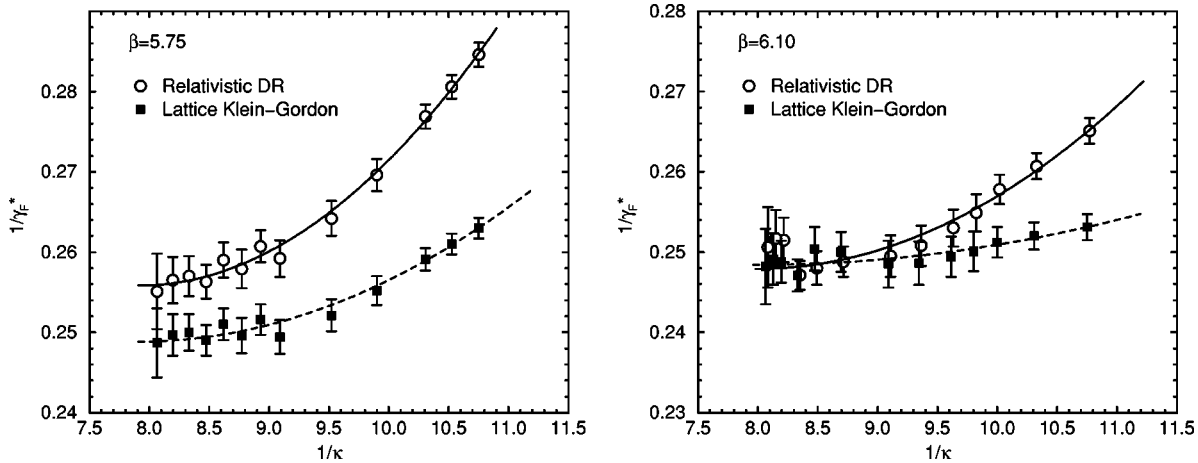

FIG. 7. Comparison of the results of calibrations with two types of dispersion relation. The curves represent the result of a linear fit in m_0^2. Solid lines are the fit results with the relativistic dispersion relation and the dashed lines are those with the lattice Klein-Gordon dispersion relation.

TABLE VI. The result of a linear fit in m_q^2 of $\gamma^*_{F(KG)}$, the tuned bare anisotropy with the Klein-Gordon dispersion relation.

β	Fit type	ζ_0	ζ_2	χ^2/N_{df}	$\gamma_F^*(m_q=0)$
5.75	linear	0.2488(8)	0.112(11)	2.33 / 11	4.019(13)
5.95	linear	0.2446(8)	0.071(14)	2.14 / 11	4.088(13)
6.10	linear	0.2484(10)	0.039(15)	1.59 / 11	4.026(16)

TABLE VII. Quark parameters used in hadron spectroscopy.

β	γ_F	Values of κ	N_{conf}
5.75	3.909	0.1240,0.1230,0.1220,0.1210	200
5.95	4.016	0.1245,0.1240,0.1235,0.1230	100
6.10	4.034	0.1245,0.1240,0.1235,0.1230	100

Uncertainty in meson mass due to calibration error

Another important issue of the systematic errors is how the uncertainty in γ_F is transmitted to the observables. As an important example, here we focus on the effect on the meson masses.

Since we linearly interpolate the meson masses in γ_F, we obtain $dm/d\gamma_F$ at $\gamma_F=\gamma_F^*$ from the slope of the linear fit. In Fig. 8, we show $dm/d\gamma_F$, the response of the meson mass to the bare anisotropy, at $\beta=6.10$ in two ways. Similar features are found in the results at $\beta=5.75$ and $\beta=5.95$. In the left panel $dm/d\gamma_F$ is shown as a function of $1/\kappa$. In the case of the vector meson, it seems to decrease linearly with increasing quark mass from zero at the massless limit. On the other hand, for the pseudoscalar meson, $dm/d\gamma_F$ is slightly positive in the vicinity of $1/\kappa_c$. This behavior may be due to the uncertainty in the definition of κ, because if κ is properly related to the fixed quark mass increasing γ_F implies increasing the propagation in the temporal direction; hence it corresponds to decreasing quark mass. Therefore, the present analysis may not be adequate for estimating the response of masses with respect to γ_F in the vicinity of the chiral limit. Observing Fig. 8, one can see that the range of quark masses larger than the strange quark mass does not suffer from the ambiguity in the definition of κ.

We have no clear explanation as to why $dm/d\gamma_F$ seems to be proportional to the quark mass. In practice, it is a good feature that the ambiguity of γ_F^* has only little effect on the meson mass in the small but nonzero quark mass region, since there a relative change of mass is significant. Except in the lightest quark mass region, the determination of γ_F^* is directly performed with 1% accuracy, which means the uncertainty of γ_F^* is around 0.04. The right panel in Fig. 8 implies that the uncertainty in the meson mass is less than 1%. This uncertainty is most severe in the heavy quark region, and becomes milder as the quark mass decreases.

While we find that the meson mass at a certain κ is not too sensitive to the uncertainty of γ_F^*, the same argument does not hold for the chiral limit. Since the pseudoscalar meson mass becomes zero in the chiral limit, the relative uncertainty $\delta m_{PS}/m_{PS}$ for a fixed κ near the chiral limit is of course very large. However, this is not the correct way to estimate the uncertainties in the mass spectrum in the chiral limit. What one is really interested in for the chiral limit is not the change in the hadron masses including the pion mass for a fixed κ but the change in the hadron masses except the pion mass at the point where the pion becomes massless. Since the critical hopping parameter κ_c is affected by the change in γ_F, one needs to treat the chiral limit carefully. In Sec. V, we discuss the uncertainties of the hadron spectrum in the chiral limit based on an extrapolation in terms of the pseudoscalar meson mass squared instead of $1/\kappa$.

D. Summary of calibration

In this section, we have implemented the anisotropic $O(a)$-improved Wilson action in the region of quark masses up to around the charm quark mass, at three values of β at $\xi=4.0$. The fermionic anisotropy ξ_F is extracted from the meson dispersion relation. Then we find the value of the bare anisotropy parameter γ_F^* at which $\xi_F=\xi$ holds. The value of γ_F^* in the massless limit is obtained by extrapolating the data by fitting to a linear form in m_q^2, where m_q is the naively defined quark mass. This is the most reliable way to deter-

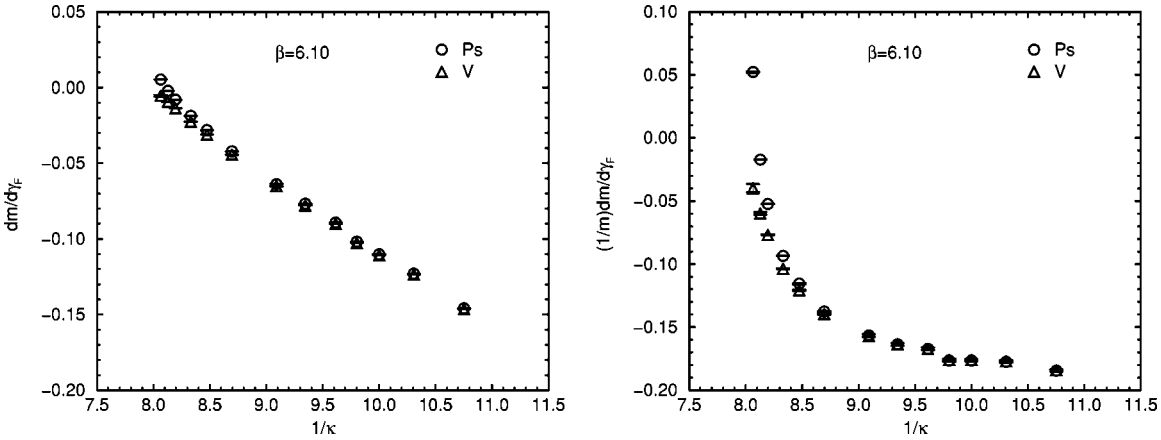

FIG. 8. The response of meson masses to a change of γ_F at $\beta=6.10$. The left panel shows $dm/d\gamma_F$, while the ratio $(1/m)dm/d\gamma_F$ is shown on the right. The results for the pseudoscalar and vector mesons are represented by circles and triangles, respectively.

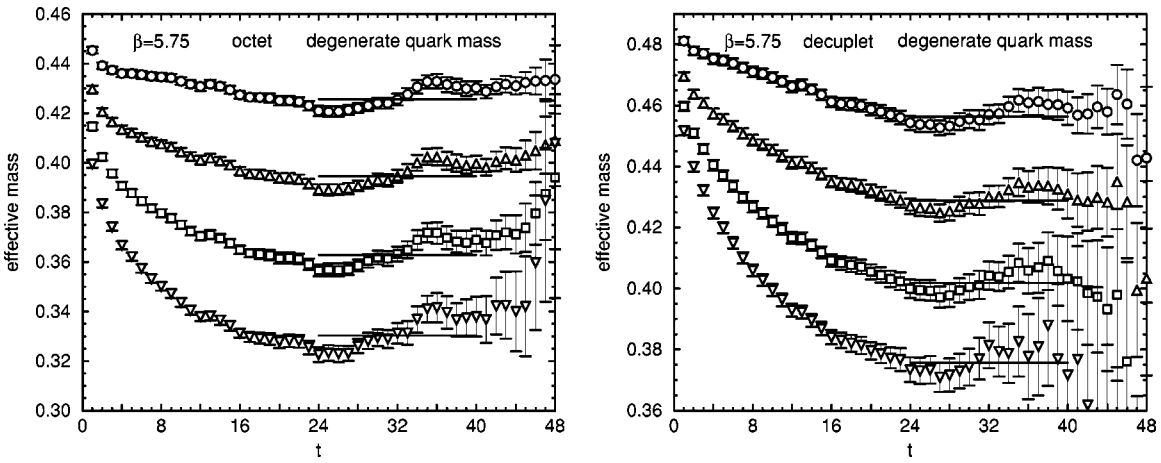

FIG. 9. Effective mass plots for octet and decuplet baryon correlators with degenerate quark masses at $\beta=5.75$. Horizontal solid line represent the fit range and the mass from the single exponential fit.

mine γ_F^* for the small quark mass region, since there the statistical fluctuation in finite momentum states is very large. The fit of $1/\gamma_F^*$ to a linear form in m_q^2 seems quite successful, and γ_F^* at the chiral limit is close to the tree-level value ξ. The statistical uncertainty in γ_F^* is estimated as on the order of 1% in the whole quark mass region explored. In the chiral limit, there is also 1% systematic uncertainty concerning the form of the fit. Here we summarize the main result of the calibration, the expression for γ_F^* at a given κ:

$$\frac{1}{\gamma_F^*}(m_q)=\zeta_0+\zeta_2 m_q^2, \qquad m_q=\frac{1}{2\xi}\left(\frac{1}{\kappa}-\frac{1}{\kappa_c}\right), \tag{4.3}$$

$$\beta=5.75:\zeta_0=0.2558(9), \quad \zeta_2=0.230(12),$$

$$\kappa_c=0.12640(5), \tag{4.4}$$

$$\beta=5.95:\zeta_0=0.2490(8), \quad \zeta_2=0.189(15),$$

$$\kappa_c=0.12592(6), \tag{4.5}$$

$$\beta=6.10:\zeta_0=0.2479(9), \quad \zeta_2=0.143(14),$$

$$\kappa_c=0.12558(4). \tag{4.6}$$

To examine the uncertainty in the calibration, we have also carried out the following analyses. (i) The difference between γ_F^* for the pseudoscalar and vector mesons, which signals the $O(\alpha a)$ systematic error. We observed that this difference decreases with decreasing lattice spacing, and is already consistent with zero at $\beta=5.95$. (ii) Comparison of γ_F^* with the continuum and the Klein-Gordon dispersion relations. This is for an estimate of the size of the $O(a^2)$ systematic uncertainty. The results with the two dispersion rela-

TABLE VIII. Hadron spectrum at $\beta=5.75$. When the quark masses are degenerate, i.e., $\kappa_1=\kappa_2$, the Σ-type and Λ-type octet baryon correlators are identical.

κ_1	κ_2	m_{PS}	m_V	$m_{oct(\Sigma)}$	$m_{oct(\Lambda)}$	m_{dec}
0.1210	0.1210	0.22909(47)	0.2821(10)	0.4257(17)	–	0.4564(24)
0.1210	0.1220	0.21716(48)	0.2730(11)	0.4146(18)	0.4161(18)	0.4472(25)
0.1210	0.1230	0.20501(51)	0.2640(12)	0.4034(19)	0.4068(19)	0.4383(27)
0.1210	0.1240	0.19260(54)	0.2552(13)	0.3920(20)	0.3977(21)	0.4299(29)
0.1220	0.1210	–	–	0.4059(19)	0.4042(19)	0.4381(27)
0.1220	0.1220	0.20480(50)	0.2637(12)	0.3946(19)	–	0.4289(28)
0.1220	0.1230	0.19214(52)	0.2546(13)	0.3831(20)	0.3852(21)	0.4199(30)
0.1220	0.1240	0.17911(55)	0.2458(15)	0.3713(21)	0.3760(22)	0.4114(33)
0.1230	0.1210	–	–	0.3863(21)	0.3820(20)	0.4202(30)
0.1230	0.1220	–	–	0.3747(22)	0.3724(21)	0.4109(32)
0.1230	0.1230	0.17886(54)	0.2454(15)	0.3629(23)	–	0.4018(35)
0.1230	0.1240	0.16503(57)	0.2364(17)	0.3506(24)	0.3538(25)	0.3932(39)
0.1240	0.1210	–	–	0.3674(25)	0.3587(22)	0.4032(37)
0.1240	0.1220	–	–	0.3555(26)	0.3490(24)	0.3938(40)
0.1240	0.1230	–	–	0.3432(27)	0.3394(25)	0.3845(44)
0.1240	0.1240	0.15015(60)	0.2272(21)	0.3303(28)	–	0.3757(51)

TABLE IX. Hadron spectrum at $\beta=5.95$.

κ_1	κ_2	m_{PS}	m_V	$m_{oct(\Sigma)}$	$m_{oct(\Lambda)}$	m_{dec}
0.1230	0.1230	0.14580(40)	0.1853(10)	0.2788(17)	–	0.3036(25)
0.1230	0.1235	0.13896(41)	0.1804(11)	0.2726(17)	0.2734(18)	0.2987(26)
0.1230	0.1240	0.13196(43)	0.1755(11)	0.2662(18)	0.2680(19)	0.2938(27)
0.1230	0.1245	0.12477(46)	0.1707(13)	0.2596(19)	0.2625(20)	0.2890(30)
0.1235	0.1230	–	–	0.2676(18)	0.2666(18)	0.2937(27)
0.1235	0.1235	0.13190(43)	0.1754(11)	0.2612(19)	–	0.2888(29)
0.1235	0.1240	0.12462(45)	0.1705(12)	0.2546(19)	0.2557(20)	0.2839(31)
0.1235	0.1245	0.11709(47)	0.1656(14)	0.2478(20)	0.2501(21)	0.2790(33)
0.1240	0.1230	–	–	0.2562(20)	0.2539(19)	0.2839(31)
0.1240	0.1235	–	–	0.2496(21)	0.2484(20)	0.2789(33)
0.1240	0.1240	0.11702(47)	0.1654(14)	0.2427(21)	–	0.2740(35)
0.1240	0.1245	0.10908(50)	0.1605(16)	0.2356(22)	0.2370(23)	0.2692(38)
0.1245	0.1230	–	–	0.2445(23)	0.2405(21)	0.2743(37)
0.1245	0.1235	–	–	0.2376(24)	0.2348(22)	0.2693(39)
0.1245	0.1240	–	–	0.2305(25)	0.2289(24)	0.2644(42)
0.1245	0.1245	0.10063(53)	0.1555(19)	0.2229(26)	–	0.2597(47)

tions tend to coincide with each other on decreasing the lattice spacing. The behavior in the large quark mass region is consistent with the expected behavior. (iii) Response of meson masses to the change of γ_F. The effect of uncertainty of γ_F^* on the meson masses is less than 1%, if γ_F^* is determined at this accuracy. This result is applicable to the relatively heavier quark mass region, such as $m_s<m_q$, and therefore in this region the errors in the calibration are under control.

V. LIGHT HADRON SPECTROSCOPY

In this section, we apply the results of the last section to the calculation of the light hadron spectrum. Our analysis is performed in two steps.

(i) By taking the central value of $\gamma_F=\gamma_F^*$ we obtain the light hadron masses in the strange quark mass region $m_s<m_q<2m_s$. By extrapolating masses in m_{PS}^2, the hadron spectrum at the physical light quark mass is determined. We compare our result with the result by the UKQCD Collaboration [15], which was obtained on an isotropic lattice with $O(a)$-improved quark action.

(ii) We study the response of the light hadron spectrum to a change of the anisotropic parameter $\gamma_F^*\to\gamma_F^*+\delta\gamma_F$. The extrapolation in m_{PS}^2 is significant in circumventing the uncertainty in the definition of κ.

A. Calculation of hadron spectrum

The spectroscopy of light hadrons is performed on the same lattices used in the calibration, but with smaller num-

TABLE X. Hadron spectrum at $\beta=6.10$.

κ_1	κ_2	m_{PS}	m_V	$m_{oct(\Sigma)}$	$m_{oct(\Lambda)}$	m_{dec}
0.1230	0.1230	0.12950(29)	0.1587(6)	0.2394(11)	–	0.2590(17)
0.1230	0.1235	0.12284(30)	0.1538(6)	0.2332(12)	0.2340(12)	0.2542(18)
0.1230	0.1240	0.11603(31)	0.1491(7)	0.2269(12)	0.2288(12)	0.2495(19)
0.1230	0.1245	0.10904(33)	0.1446(8)	0.2204(13)	0.2236(13)	0.2451(21)
0.1235	0.1230	–	–	0.2283(12)	0.2273(12)	0.2493(19)
0.1235	0.1235	0.11595(31)	0.1489(7)	0.2219(13)	–	0.2445(20)
0.1235	0.1240	0.10886(32)	0.1442(8)	0.2154(13)	0.2166(13)	0.2399(22)
0.1235	0.1245	0.10153(33)	0.1398(9)	0.2087(14)	0.2112(14)	0.2355(24)
0.1240	0.1230	–	–	0.2171(14)	0.2148(13)	0.2400(22)
0.1240	0.1235	–	–	0.2106(14)	0.2093(14)	0.2352(24)
0.1240	0.1240	0.10142(33)	0.1395(8)	0.2038(14)	–	0.2306(26)
0.1240	0.1245	0.09366(35)	0.1352(10)	0.1968(15)	0.1983(16)	0.2263(30)
0.1245	0.1230	–	–	0.2058(16)	0.2017(15)	0.2314(28)
0.1245	0.1235	–	–	0.1990(16)	0.1960(15)	0.2267(30)
0.1245	0.1240	–	–	0.1919(17)	0.1903(16)	0.2221(34)
0.1245	0.1245	0.08535(36)	0.1310(12)	0.1845(18)	–	0.2180(41)

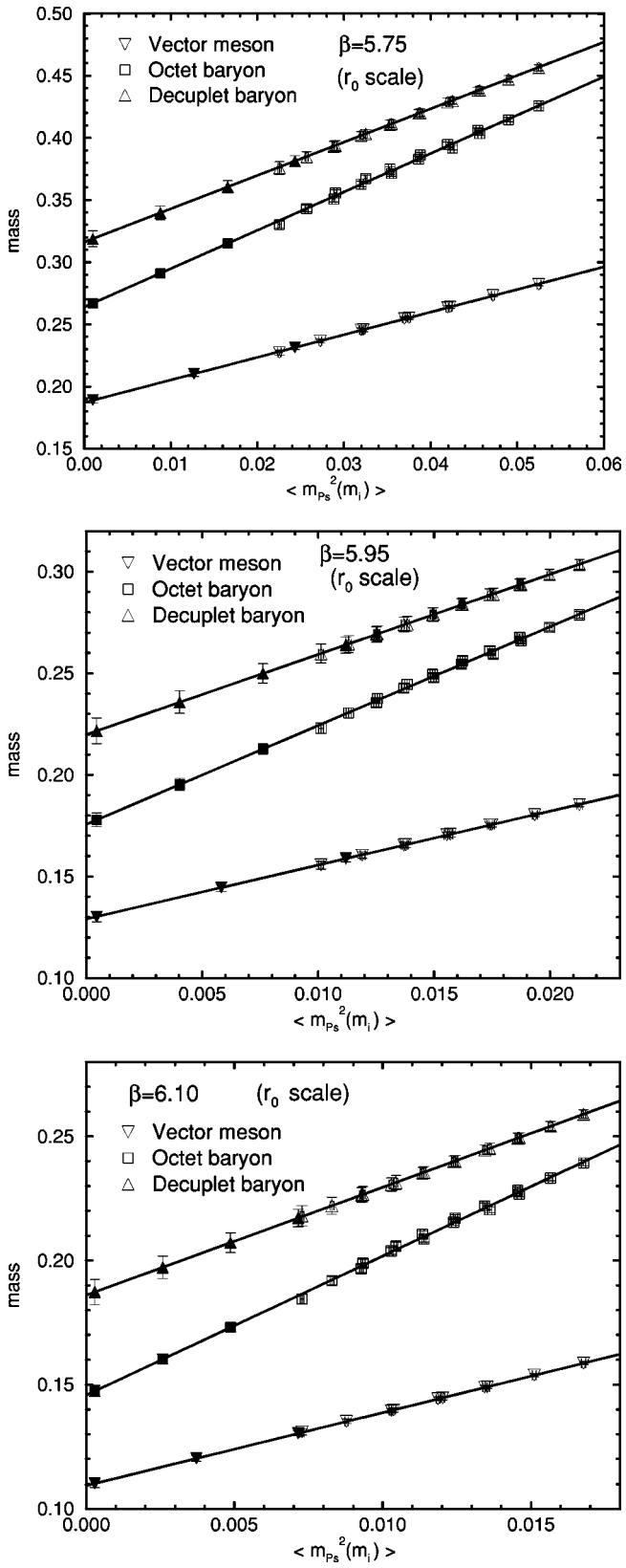

FIG. 10. The masses of vector mesons and octet and decuplet baryons together with the result of linear fits. Only the Σ-type octet baryon is shown. The filled symbols correspond to the masses at the physical *u, d,* and *s* quark masses with the scale set by r_0.

bers of configurations. The parameters are listed in Table VII. At each β, we use four values of κ corresponding to the quark masses m_s-2m_s. In this region, we consider that m_q is sufficiently small so that we can adopt the value of γ_F^* in the massless limit. Therefore the bare anisotropy is set to the central value of γ_F^* at $m_q=0$, which is determined in the calibration as the linear form in m_q^2.

We use the standard hadron operators and procedure to extract the hadron masses. The quark propagators are smeared at the source with a Gaussian smearing function with the deviation $\simeq 0.4$ fm in the Coulomb gauge. The periodic boundary condition is adopted in all four directions for the quark field. For baryons, two of the quarks are treated as having degenerate masses. Then the quark content of the baryons is specified by two κ's, κ_1 and κ_2, for a pair of quarks and the other quark, respectively. Figure 9 shows the effective mass plot for octet and decuplet baryons with degenerate quark masses $\kappa_1=\kappa_2$. The meson correlators are fitted to a single hyperbolic cosine form. For baryons, we apply a single exponential fit in the region in which there is negligible contribution of the negative parity baryon from the other temporal boundary. The results of the fit are listed in Tables VIII–X. For mesons, since the order of κ_1 and κ_2 is unimportant, the masses for the exchanged set of (κ_1,κ_2) are omitted. The masses of the Λ-type octet baryons at degenerate (κ_1,κ_2) are also omitted, since they are identical to the masses of the Σ type.

B. Extrapolation to the chiral limit

In order to avoid ambiguities in the definition of the quark mass, we extrapolate the hadron masses to the chiral limit in terms of the pseudoscalar meson mass squared, instead of $1/\kappa$. We assume the relation

$$m_{PS}^2(m_1,m_2)=B(m_1+m_2); \tag{5.1}$$

then for degenerate quark masses $m_1=m_2$ $m_{PS}^2=2Bm_1$ holds. Then instead of m_i $(i=1,2)$, one can use $m_{PS}(m_i,m_i)^2$ as the variable in the chiral extrapolation. For other hadrons, vector mesons and octet and decuplet baryons, we also use the linear relations

$$m_V(m_1,m_2)=m_V(0,0)+B_V(m_1+m_2), \tag{5.2}$$

$$m_{oct}(m_1,m_2,m_3)=m_{oct}(0,0,0)+B_{oct}(m_1+m_2+m_3), \tag{5.3}$$

$$m_{dec}(m_1,m_2,m_3)=m_{dec}(0,0,0)+B_{dec}(m_1+m_2+m_3). \tag{5.4}$$

The hadron spectrum and the result of the fit are shown in Fig. 10. The horizontal axis is the averaged pseudoscalar meson mass squared:

$$\langle m_{PS}^2(m_i)\rangle=\frac{1}{N_q}\sum_{i=1}^{N_q} m_{PS}^2(m_i,m_i)=\frac{1}{N_q}\sum_{i=1}^{N_q} 2Bm_i \tag{5.5}$$

TABLE XI. Hadron spectrum for physical quark masses with the scale set by r_0.

	Mass (GeV)			$m\xi r_0$			Ref. [15]
	$\beta=5.75$	$\beta=5.95$	$\beta=6.10$	$\beta=5.75$	$\beta=5.95$	$\beta=6.10$	cont.
ρ	0.832(11)	0.846(17)	0.895(12)	2.105(28)	2.141(42)	2.265(30)	2.35(16)
K^*	0.9251(90)	0.938(13)	0.977(10)	2.342(23)	2.375(34)	2.473(25)	2.54(12)
ϕ	1.0185(71)	1.031(10)	1.059(8)	2.578(18)	2.610(26)	2.680(21)	2.729(77)
N	1.175(16)	1.155(22)	1.197(18)	2.974(40)	2.924(55)	3.032(45)	2.92(24)
Λ	1.260(13)	1.253(19)	1.283(16)	3.190(34)	3.172(47)	3.248(40)	3.22(20)
Σ	1.281(14)	1.268(19)	1.302(16)	3.242(35)	3.211(49)	3.295(41)	3.23(19)
Ξ	1.387(12)	1.381(17)	1.406(15)	3.510(31)	3.497(43)	3.558(37)	3.54(15)
Δ	1.403(28)	1.440(41)	1.521(41)	3.552(72)	3.65(10)	3.85(10)	3.86(37)
Σ^*	1.495(25)	1.532(36)	1.602(37)	3.784(63)	3.877(90)	4.055(93)	4.15(29)
Ξ^*	1.587(22)	1.623(31)	1.683(32)	4.017(54)	4.109(78)	4.260(81)	4.44(22)
Ω	1.679(18)	1.715(26)	1.763(28)	4.249(46)	4.341(66)	4.464(70)	4.72(17)

with $N_q=2$ for mesons and $N_q=3$ for baryons. The Λ-type baryon is not shown in the figure for clarity. The linear fit seems to be successful.

C. Spectrum at physical quark masses

To determine the hadron masses at the physical u, d, and s quark masses, one needs to set the scale of the lattice. We do not distinguish the u and d quark masses, and express their mass as m_n. We adopt two definitions, through the hadronic radius r_0, and through the K^* meson mass. These two methods were also adopted by the UKQCD Collaboration in [15], and are convenient for comparison of our data with theirs. In [15], values of the clover coefficient were determined in two ways: by a nonperturbative renormalization technique (NP) [16], and tadpole improvement (TAD) [12]. Then the masses were extrapolated to the continuum limit by a simultaneous fit of these two types of data to a linear form in a^2 for NP and a quadratic form in a for TAD. We compare our hadron spectrum at the physical quark masses with the result in the continuum limit of [15], although we ourselves do not perform the continuum extrapolation because of a lack of sufficient numbers of β as well as the statistical accuracy.

Scale set by r_0

The hadronic radius r_0 has already been obtained in Sec. IV. The corresponding values of spatial lattice cutoff are found in Table I. The PS meson masses squared corresponding to m_n and m_s are then defined by $m_\pi^\pm=139.6$ MeV and $m_K=495.7$ MeV (isospin averaged), respectively. These definitions are in accord with [15]. The hadron masses extrapolated or interpolated to the physical points are shown in Fig. 10 and listed in Table XI. For comparison with the results in [15], we also list the hadron masses multiplied by $r_0\xi$ in Table XI. In the latter case, ξ appears to convert a quantity in spatial lattice units (r_0) to one in temporal lattice units (masses). In our data, differences between the results at $\beta=6.10$ and 5.95 are rather large compared with the differences between $\beta=5.95$ and 5.75. This would be partially due to the different a dependence of the $O(\alpha a)$ and $O(a^2)$ lattice

TABLE XII. Hadron spectrum for physical quark masses with the scale set by m_{K^*}. The parameter J is also quoted; while it is dimensionless quantity.

	Mass (GeV)			m/m_{K^*}			Ref. [15]
	$\beta=5.75$	$\beta=5.95$	$\beta=6.10$	$\beta=5.75$	$\beta=5.95$	$\beta=6.10$	cont.
ρ	0.796(11)	0.795(16)	0.802(11)	0.891(12)	0.890(18)	0.898(12)	$0.921(^{+32}_{-56})$
K^*	0.894(11)	0.894(16)	0.894(11)	–	–	–	–
ϕ	0.992(12)	0.993(16)	0.986(11)	1.109(13)	1.110(18)	1.103(12)	$1.110(^{+8}_{-21})$
N	1.125(15)	1.087(21)	1.075(16)	1.259(17)	1.216(23)	1.202(18)	$1.14(^{+6}_{-18})$
Λ	1.217(14)	1.194(20)	1.175(15)	1.361(15)	1.335(22)	1.315(17)	$1.29(^{+5}_{-15})$
Σ	1.236(14)	1.207(20)	1.191(16)	1.382(16)	1.351(23)	1.332(17)	$1.29(^{+5}_{-14})$
Ξ	1.346(14)	1.328(21)	1.307(15)	1.506(16)	1.485(23)	1.462(17)	$1.45(^{+4}_{-10})$
Δ	1.343(27)	1.354(39)	1.363(37)	1.502(30)	1.515(43)	1.525(41)	$1.50(^{+17}_{-17})$
Σ^*	1.439(25)	1.452(35)	1.454(33)	1.610(28)	1.624(39)	1.626(37)	$1.64(^{+13}_{-13})$
Ξ^*	1.535(23)	1.549(32)	1.544(29)	1.717(25)	1.733(36)	1.727(32)	$1.79(^{+9}_{-10})$
Ω	1.631(21)	1.647(30)	1.634(25)	1.825(24)	1.842(33)	1.828(28)	$1.93(^{+7}_{-8})$
J	0.3859(47)	0.3896(95)	0.3621(47)				

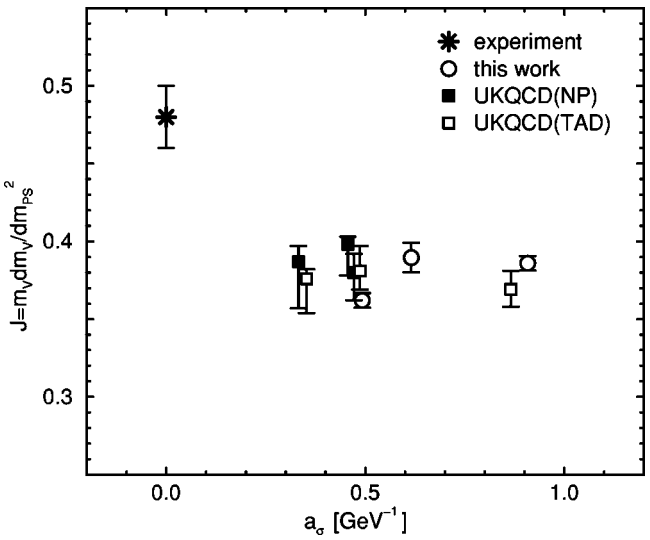

FIG. 11. The parameter J. The a_σ is set by using r_0. Data from UKQCD Collaboration (square symbols) are taken from Ref. [15] on isotropic lattices, and slightly horizontally shifted.

artifacts, and also due to the statistical fluctuation. Our results for the hadron masses seem to approach the continuum results of the UKQCD Collaboration on an isotropic lattice [15].

Scale set by m_{K^*}

In the second case, $m_{K^*}=893.9$ MeV (isospin averaged) is used to set the lattice scale. First we interpolate the vector meson mass to the point where the ratio of PS and V meson masses is equal to the ratio of the physical values of K^* and K mesons. Then this vector meson mass defines the lattice scale. This results in the spatial lattice cutoffs 1.053(13), 1.525(27), and 1.817(22) GeV at $\beta=5.75$, 5.95, and 6.10, respectively. Then the values of m_{PS}^2 corresponding to the (u,d) and s quark masses are determined with the experimental K and π meson masses. The hadron masses at physical quark masses are listed in Table XII. We observe a similar tendency to that when the scale is set by r_0. No signal of inconsistency with the results on the isotropic lattice is found.

D. J parameter

The parameter J was introduced to probe the quenching effect in [17], and defined as

$$J=m_V\frac{dm_V}{dm_{PS}^2}\bigg|_{m_V/m_{PS}=m_{K^*}/m_K}. \tag{5.6}$$

It is known that the quenched lattice simulation does not reproduce the experimental value $J=0.48(2)$; it gives an about 20% smaller value. We show our result for J in Fig. 11, as a function of lattice spacing determined by r_0. We find that our results are consistent with those of the UKQCD Collaboration on isotropic lattices in the quenched approximation.

E. Covariance of correlators

Let us consider the pseudoscalar correlator

$$C_{PS}(\boldsymbol{p},t)=\langle O_{PS}(x)O_{PS}^\dagger(0)\rangle \rightarrow Z^2(\boldsymbol{p})\exp[-E(\boldsymbol{p})t] \quad (\text{large } t) \tag{5.7}$$

with $Z(\boldsymbol{p})=\langle 0|O(x)|PS(\boldsymbol{p})\rangle/\sqrt{2E(\boldsymbol{p})}$. Here we employ the covariant normalization. For the local pseudoscalar density operator $O(x)=\overline{q}(x)\gamma_5 q(x)$, if Lorentz covariance is sufficiently restored, $Z(\boldsymbol{p})\sqrt{2E(\boldsymbol{p})}$ does not depend on the momentum $\boldsymbol{p}$. Then

$$R(\boldsymbol{p})=\frac{E(\boldsymbol{p})Z(\boldsymbol{p})^2}{m_{PS}Z(0)^2} \tag{5.8}$$

probes the restoration of covariance as a deviation from unity. In Fig. 12, we show the momentum dependence of $R(\boldsymbol{p})$ measured for $\beta=5.95$ and 6.10. At each β, the quark

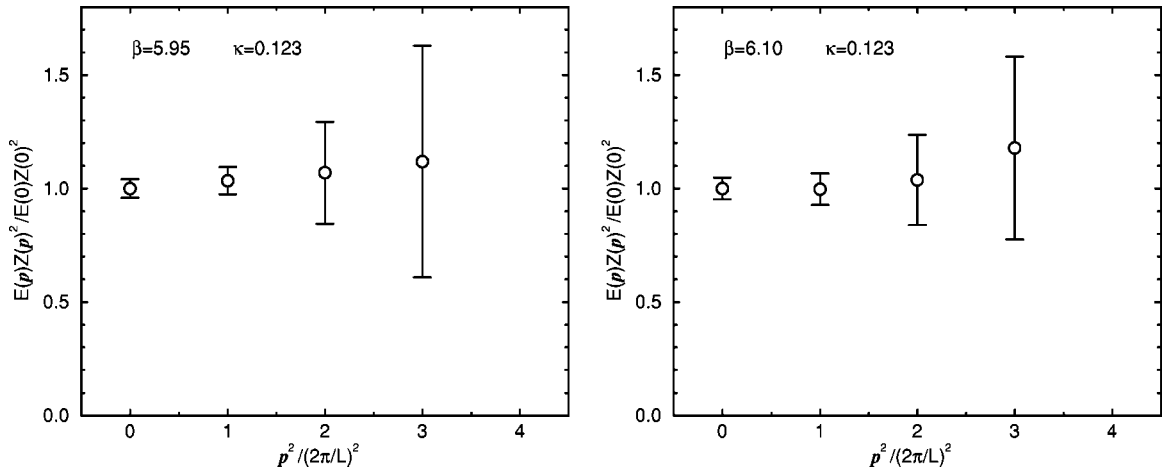

FIG. 12. The covariance of the pseudoscalar correlators. The left panel is at $\beta=5.95$ and $\kappa=0.1230$, and the right at $\beta=6.10$ and $\kappa=0.1230$.

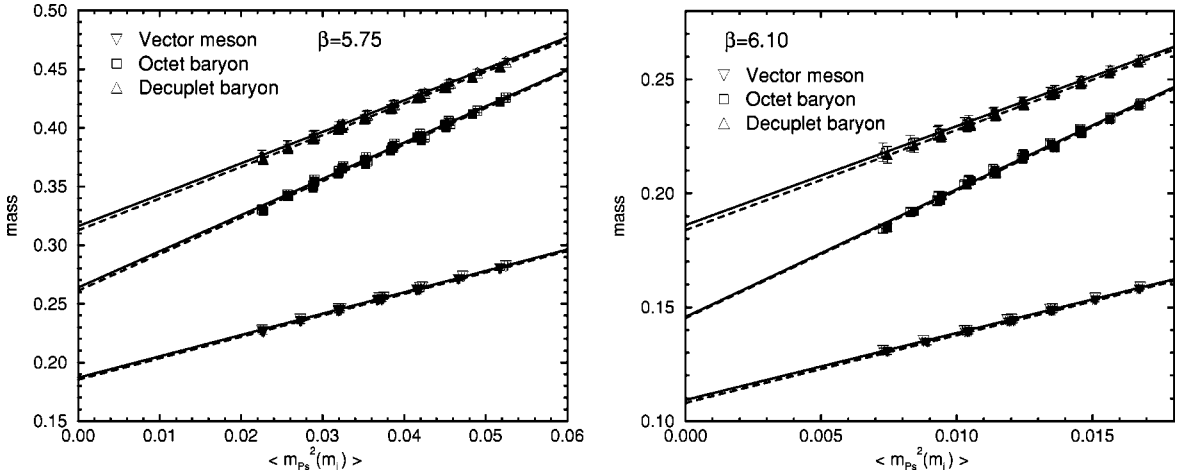

FIG. 13. The spectra with shifted γ_F (filled symbols) together with the results at γ_F^* (open symbols). The solid lines and dashed lines represent the fit results at $\gamma_F=\gamma_F^*$ and $\gamma_F^*+\delta\gamma_F$, respectively.

mass is the largest one used in the light hadron spectroscopy. We find that $R(\boldsymbol{p})$ at finite momentum is consistent with $R(\boldsymbol{p}=\boldsymbol{0})$, while higher momentum states suffer from large statistical fluctuation. This feature is particularly important in the calculation of form factors, in which the finite momentum states play an essential role.

F. Systematic errors of the spectrum from calibration

To estimate the systematic effect due to the uncertainty of calibration, we obtain the spectrum at the same κ's with slightly shifted bare anisotropy $\gamma_F'=\gamma_F^*+\delta\gamma_F$. We set $\delta\gamma_F=0.1$, which implies about 2.5% shift of the bare anisotropy. Figure 13 shows the result for shifted γ_F together with the result for γ_F^*, for $\beta=5.75$ and 6.10. There are small systematic downward shifts in the fitted lines. The spectra at the physical quark masses are listed in Table XIII as the dimensionless combinations $m\xi r_0$ and m/m_{K^*}. The difference between the masses with γ_F' and γ_F^* is slightly amplified toward the chiral limit. Even for the lightest mass in each species, the difference is at most around 1%. This implies that the uncertainties of the hadron masses at the physical (u,d) and s quark masses are about half the uncertainty in γ_F. With the relativistic dispersion relation, γ_F^* at $m_q=0$ has been determined at each β within about 2% ambiguity: the statistical error of 1% and the systematic error of 1% in the form of the fit. Therefore there is 1% level uncertainty in the hadron spectrum due to the uncertainty in calibration. This feature makes the anisotropic lattice promising for future physical applications.

VI. CONCLUSION

In this paper, we studied the $O(a)$ improved quark action on an anisotropic lattice with anisotropy $\xi=a_\sigma/a_\tau=4$. The bare anisotropy γ_F^*, for which $\xi_F=\xi$ holds, is determined for the whole quark mass region below the charm quark mass, including the chiral limit, at 1% statistical accuracy. In the massless limit, there is also about 1% systematic uncertainty in extrapolating γ_F^* to $m_q=0$.

TABLE XIII. Spectra with shifted γ_F in dimensionless combinations. The dimensionless parameter J is also listed.

	$m\xi r_0$			m/m_K^*		
β	5.75	5.95	6.10	5.75	5.95	6.10
ρ	2.084(26)	2.121(40)	2.239(28)	0.891(11)	0.890(17)	0.898(11)
K^*	2.322(21)	2.357(32)	2.448(24)	–	–	–
ϕ	2.560(17)	2.592(24)	2.658(19)	1.109(12)	1.110(17)	1.102(12)
N	2.946(37)	2.913(52)	3.019(43)	1.260(16)	1.223(22)	1.212(17)
Λ	3.166(32)	3.161(45)	3.236(38)	1.363(15)	1.341(21)	1.323(16)
Σ	3.216(33)	3.199(46)	3.282(39)	1.383(15)	1.356(22)	1.340(17)
Ξ	3.486(29)	3.485(41)	3.545(35)	1.507(15)	1.490(22)	1.468(17)
Δ	3.514(66)	3.614(96)	3.808(96)	1.503(28)	1.517(41)	1.527(38)
Σ^*	3.748(58)	3.847(85)	4.014(85)	1.610(26)	1.625(37)	1.627(34)
Ξ^*	3.983(50)	4.080(73)	4.221(75)	1.717(24)	1.734(34)	1.728(30)
Ω	4.217(43)	4.313(62)	4.427(65)	1.824(23)	1.842(32)	1.829(27)
J				0.3838(43)	0.3871(86)	0.3614(42)

The uncertainties in the calibration due to the discretization errors are studied by changing the physical inputs or conditions. (i) We have shown that the dispersion relations for the pseudoscalar and vector mesons give values of γ_F^* that differ by 1% at $\beta=5.75$, while they show no difference at $\beta=5.95$ and 6.10. (ii) Two different choices of the lattice dispersion relation, namely, the naive continuum form and the Klein-Gordon form, also lead to results that differ by 3% for $\beta=5.75$, but we found no difference at $\beta=6.1$ with $m_q < 0.2a_\tau^{-1}$. These systematic uncertainties tend to vanish toward the continuum limit.

The light hadron spectrum was studied using the central value of the tuned bare anisotropy $\gamma_F^*(m_q=0)$. We found that it is consistent with the result on the isotropic lattice obtained by the UKQCD Collaboration. It was found that a change of γ_F^* by 2% would lead to a change of the spectrum by 1% for the physical quark masses. We also investigated the Lorentz invariance of the matrix element of the pseudoscalar operator as a consistency check.

The main disadvantage in using the anisotropic lattice would lie in the additional systematic uncertainty caused by the calibration. There are two types of error in γ_F^*. The first type consists of the statistical error and the error in the chiral extrapolation, which was estimated to be at the 2% level. The second type consists of $O(\alpha a)$ and $O(a^2)$ systematic uncertainties, which were estimated to be 4% at $\beta=5.75$ and smaller for larger β. In total, there is 6% ambiguity at $\beta=5.75$, which corresponds to our coarsest lattice, and 2–3 % ambiguity at $\beta=6.10$. The relative errors in the hadron spectrum are half of those in γ_F^*. Since the contribution from the second type of error vanishes in the continuum limit, we expect to obtain the hadron spectrum to 1% accuracy in the continuum limit. This result is encouraging for further applications. The anisotropic lattice would already be applicable to quantitative studies that require a few percent accuracy. To achieve higher accuracy, nonperturbative tuning of the clover coefficients is required.

Since the range of quark masses where the systematic errors are under control covers the charm quark region, it is also important to apply the present anisotropic lattice simulation to the charmonium and D meson systems.

ACKNOWLEDGMENTS

We thank J. Harada, A. S. Kronfeld, O. Miyamura, N. Nakajima, Y. Nemoto, H. Suganuma, and T. T. Takahashi for useful discussions. The simulation was done on a NEC SX-5 at the Research Center for Nuclear Physics, Osaka University and a Hitachi SR8000 at KEK (High Energy Accelerator Research Organization). H.M. was supported by the Japan Society for the Promotion of Science for Young Scientists and also in the early stage of this work by the center-of-excellence (COE) program at RCNP, Osaka University. T.O. was supported by a Grant-in-Aid of the Ministry of Education No. 12640279. T.U. was supported by the center-of-excellence (COE) program at CCP, Tsukuba University.

[1] F. Karsch, Nucl. Phys. **B205**, 285 (1982).
[2] G. Burgers, F. Karsch, A. Nakamura, and I.O. Stamatescu, Nucl. Phys. **B304**, 587 (1988).
[3] QCD-TARO Collaboration, M. Fujisaki *et al.* Nucl. Phys. B (Proc. Suppl.) **53**, 426 (1997).
[4] F. Karsch, J. Engels, and T. Scheideler, Nucl. Phys. B (Proc. Suppl.) **63**, 427 (1998); J. Engels, F. Karsch, and T. Scheideler, Nucl. Phys. **B564**, 303 (2000).
[5] T.R. Klassen, Nucl. Phys. **B533**, 557 (1998).
[6] T. Umeda, R. Katayama, O. Miyamura, and H. Matsufuru, Int. J. Mod. Phys. A **16**, 2215 (2000).
[7] T.R. Klassen, Nucl. Phys. B (Proc. Suppl.) **73**, 918 (1999).
[8] P. Chen, Phys. Rev. D **64**, 034504 (2001).
[9] CP-PACS Collaboration, A. Ali Khan *et al.*, Nucl. Phys. B (Proc. Suppl.) **94**, 325 (2001).
[10] J. Harada, A. S. Kronfeld, H. Matsufuru, N. Nakajima, and T. Onogi, Phys. Rev. D **64**, 074501 (2001).
[11] A.X. El-Khadra, A.S. Kronfeld, and P.B. Mackenzie, Phys. Rev. D **55**, 3933 (1997).
[12] G.P. Lepage and P.B. Mackenzie, Phys. Rev. D **48**, 2250 (1993).
[13] B.A. Thacker and G.P. Lepage, Phys. Rev. D **43**, 196 (1991).
[14] R. Sommer, Nucl. Phys. **B411**, 839 (1994).
[15] UKQCD Collaboration, K.C. Bowler *et al.*, Phys. Rev. D **62**, 054506 (2000).
[16] M. Lüscher, S. Sint, R. Sommer, P. Weisz, and U. Wolff, Nucl. Phys. **B491**, 323 (1997).
[17] UKQCD Collaboration, P. Lacock and C. Michael, Phys. Rev. D **52**, 5213 (1995).